Guidance Characteristics of Two-Dimensionally Periodic Impedance Surface

Ruey Bing Hwang, *Member, IEEE,* and Song Tsuen Peng, *Fellow, IEEE*

***Abstract*— In this paper, we present an exact formulation for the three-dimensional boundary-value problem of waveguiding by a two-dimensional periodic impedance surface in a uniform medium. The dispersion characteristics of such a structure are rigorously analyzed in terms of the complete set of both TE- and TM-polarized plane waves in the uniform medium. The results are systematically expressed in the form of the Brillouin diagram; thereby, in comparison to the one-dimensional case, a host of new and interesting phenomena are identified and physically explained.**

***Index Terms*— Bandgap, stopband, surface wave, two-dimensional periodic impedance surface, two-dimensional periodic structures.**

I. Introduction

THE guiding of waves by periodic structures has long been a subject of continuing interest, and extensive theoretical and experimental results are available in the literature [1]–[10]. While most of the work in the past had been limited to the one-dimensional (1-D) case, the class of two-dimensional (2-D) periodic structures has attracted considerable attention in recent years; in some applications, they have been referred to as photonic-bandgap structures [11]–[17]. For example, for microwave and millimeter-wave circuit and antenna applications [13]–[17], periodic structures have been utilized for performing the key function of suppressing leaky surface waves. These structures can be fabricated with relative ease and should find many applications in practice. Although the special case of bigrating structures has been extensively investigated and well understood [18]–[21], most of the work had been limited to experimental studies and simulations using different numerical methods. While the type of research is needed for developing design rules that are useful for practical considerations, a clear physical picture of wave processes is desirable for understanding the wave phenomena in 2-D periodic structures. The goal of this paper is to build up fundamental understanding of waves guided on the 2-D periodic impedance surface and to explore new and interesting phenomena that are not realized in the 1-D case.

Specifically, we consider the guiding of waves by an impedance surface that is periodic in two dimensions. This class of structures is intended as a model for the study of wave propagation in 2-D periodic structures. In fact, the case of 1-D periodic reactive surface [2] had been employed successfully as a model for the analysis of wave phenomena associated with periodic structures; for the first time, Wood's anomaly was then explained on a rigorous basis. We have observed that the case of 2-D periodic impedance surface can be formulated rigorously by the method of mode matching as a three-dimensional electromagnetic boundary value problem. The total fields above the planar impedance surface can be expressed in the form of double Fourier series, with each space harmonic appearing as a plane wave consisting of both TE and TM polarized constituent ones. The condition for the existence of a nontrivial solution in the absence of incident wave yields the dispersion relation of the waveguiding structure; thus, this problem is considered completely solved.

Based on the exact approach described above, we have carried out extensive numerical results to identify and explain physical phenomena associated with the 2-D periodic impedance surface. The dispersion characteristics of 2-D periodic structures are displayed in the form of the Brillouin diagram, with both phase and attenuation constants included. In particular, the bound-wave regions are carefully examined, and very interesting numerical results are obtained, exhibiting some extraordinary dispersion characteristics that cannot take place in the case of 1-D periodic structures. In short, the results establish considerable distinctive characteristics of the 2-D periodic structures.

II. Statement of Problem

Fig. 1(a) depict the scattering of a plane wave by a planar impedance surface that is periodic in two dimensions. The dispersion relation of such an impedance surface can then be obtained from the resonance of the scattering problem. This defines the relation between k_x and k_y, so that if one of them is given, the other is then determined. For example, consider the case shown in Fig. 1(b), where a 2-D periodic impedance surface is connected to a uniform impedance surface at $x = 0$ (along the y-axis), and a surface wave is incident obliquely from the uniform impedance surface at the angle ϕ_{inc}. Here, by fixing the incident angle, k_y is determined for a given frequency and we can look for the dispersion root of k_x. For simplicity, the space above the surface is taken to be air of infinite extent; otherwise, this can always be done by an appropriate normalization. Such a structure is intended as a model for the study of wave phenomena associated with the class of multilayer periodic structures. In the literature, the case of 1-D periodic reactive surface had been successfully

Manuscript received March 26, 1999; revised July 16, 1999. This work was supported in part by the National Science Council under Contract NSC 89-2213-E009-074, and by the Telecommunication Laboratories, ChungHwa Telcom Company Ltd. under Contract TL-88-2201.

The authors are with the Microelectronic and Information Systems Research Center, National Chiao Tung University, Hsinchu, Taiwan, ROC.

Publisher Item Identifier S 0018-9480(99)08448-3.

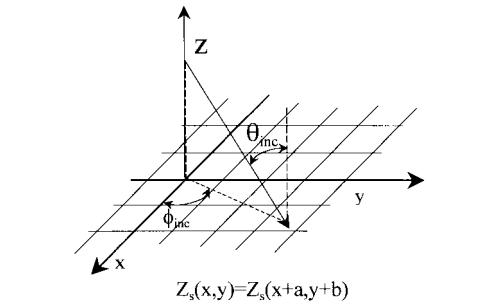

(a)

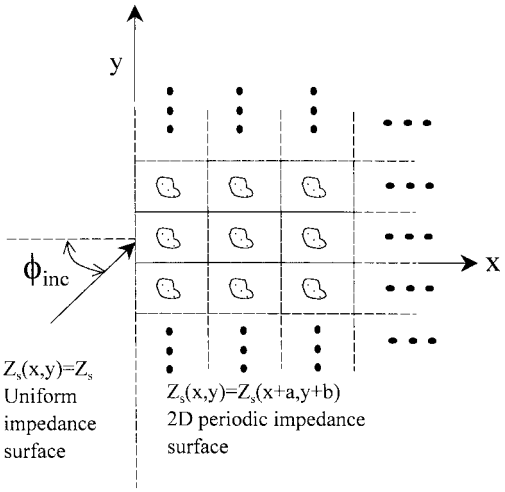

(b)

Fig. 1. Scattering and guidance of plane wave by a 2-D periodic impedance surface. (a) Scattering by plane wave. (b) Surface wave obliquely incident.

employed as a model for the analysis of wave phenomena associated with periodic structures; for the first time, the Wood's anomaly was explained on a rigorous basis [2]. As an extension, we consider here a periodically perturbed surface impedance with the spatial variation given by

$$Z(x,y) = Z_s\left[1 + 2\delta_x \cos\frac{2\pi x}{a} + 2\delta_y \cos\frac{2\pi y}{b} + 4\delta_{xy}\cos\frac{2\pi x}{a}\cos\frac{2\pi y}{b}\right] \quad (1)$$

$$Z_s = R_s + jX_s. \quad (2)$$

Here, Z_s is the average surface impedance, with the surface resistance R_s, and the surface reactance X_s; δ_x, δ_y, and δ_{xy} are the modulation indexes; and a and b are the periods in the x- and y-direction, respectively. Such a characterization may be regarded as the first-order approximation of a Fourier series for a general 2-D periodic surface impedance; if needed, more terms may be included and the ensuing analysis can be applied with only some slight modifications. We begin the formulation with the scattering of plane waves for the sake of generality; the guiding of waves by the structure can then be treated naturally by the technique of transverse resonance, as explained in Section III.

III. Method of Analysis

Referring to Fig. 1(a), an incident plane wave is scattered by the 2-D periodic impedance surface and a set of space harmonics in each of the two directions of periodic variations is generated. In the air region, each space harmonic appears as a plane wave, which may be generally represented as a superposition of the TE- and TM-polarized constituent plane waves. For the mnth harmonics, the tangential-field components can be written as

$$\underline{z}_o \times \underline{E}_{tmn}(\underline{\rho}, z) = \left[\underline{a}'_{mn} V'_{mn}(z) + \underline{a}''_{mn} V''_{mn}(z)\right] \cdot \exp(-j\underline{k}_{tmn}\cdot\underline{\rho}) \quad (3)$$

$$\underline{H}_{tmn}(\underline{\rho}, z) = \left[\underline{a}'_{mn} I'_{mn}(z) + \underline{a}''_{mn} I''_{mn}(z)\right] \cdot \exp(-j\underline{k}_{tmn}\cdot\underline{\rho}). \quad (4)$$

In these equations, the single and double primes denote the TE- and TM-polarized waves, respectively. $\underline{\rho}$ stands for the transverse coordinate vector, while the z-axis is taken as the longitudinal direction. $\underline{a}'_{mn}$ and $\underline{a}''_{mn}$ are mutually perpendicular 2-D unit vectors that are related to the transverse propagation vector, $\underline{k}_{tmn}$ by

$$\underline{a}'_{mn} = \frac{\underline{k}_{tmn}}{k_{tmn}} \quad (5a)$$

$$\underline{a}''_{mn} = \underline{z}_o \times \underline{a}'_{mn} = \frac{\underline{z}_o \times \underline{k}_{tmn}}{k_{tmn}} \quad (5b)$$

with

$$\underline{k}_{tmn} = k_{xm}\underline{x}_o + k_{yn}\underline{y}_o \quad (6a)$$

$$k_{xm} = k_x + \frac{2m\pi}{a} \quad (6b)$$

$$k_{yn} = k_y + \frac{2n\pi}{b}. \quad (6c)$$

Here, k_{xm} and k_{yn} are the propagation constants of the mth space harmonic in the x-direction and the nth space harmonic in the y-direction, respectively. It is noted that in the expressions above, we have defined the symbols $\underline{x}_o$, $\underline{y}_o$, and $\underline{z}_o$ for the three unit base vectors of the rectangular coordinate system. Furthermore, the V's and I's represent the vertical variations of the electric and magnetic fields of the mnth harmonics, respectively, and can be written generally as a superposition of the forward and backward traveling waves as

$$V_{mn}(z) = V_{mn}^{(+)}\exp(-jk_{zmn}z) + V_{mn}^{(-)}\exp(+jk_{zmn}z) \quad (7)$$

$$I_{mn}(z) = Y_{mn}\left[V_{mn}^{(+)}\exp(-jk_{zmn}z) - V_{mn}^{(-)}\exp(+jk_{zmn}z)\right] \quad (8)$$

where $V_{mn}^{(+)}$ and $V_{mn}^{(-)}$ are the amplitudes of the forward and backward traveling waves, respectively. It is noted that the primes over the V's and I's are omitted here for simplicity; these expressions hold for either singly or doubly primed quantities, denoting the TE- and TM-polarized fields. Finally, the longitudinal propagation constant k_{zmn} and the wave admittance Y_{mn} of the mnth harmonic in the air region are defined by

$$k_{xm}^2 + k_{yn}^2 + k_{zmn}^2 = k_o^2 \quad (9)$$

and

$$Y_{mn} = \begin{cases} Y'_{mn} = \dfrac{k_{zmn}}{\omega\mu_o} \\ Y''_{mn} = \dfrac{\omega\varepsilon_o}{k_{zmn}} \end{cases} \tag{10}$$

where k_o, μ_o, and ε_o are, respectively, the wavenumber, permeability, and permittivity of the free space. For the scattering of a plane wave by the 2-D periodic impedance surface, k_x and k_y in (6) are supposed to be known. Up to this point, the amplitudes of the forward and backward traveling waves $V_{mn}^{(+)}$ and $V_{mn}^{(-)}$ for $m, n = \cdots, -1, 0, 1, \cdots$, are the only unknown quantities remaining to be determined.

The total electromagnetic fields in the air region can be represented as a superposition of those of the space harmonics given in (3) and (4), and they are required to satisfy the boundary condition at the periodic impedance surface at the plane $z = 0$

$$\underline{z}_o \times \underline{E}(\underline{\rho}, 0) = Z_s(x, y)\underline{H}(\underline{\rho}, 0). \tag{11}$$

In the Appendix, it is shown in mathematical details that in the absence of incident wave, the boundary condition above yields a set of vector recurrence relations for the Fourier amplitudes as

$$\mathbf{A}_{m+1}\underline{I}_{m+1} + \mathbf{D}_m\underline{I}_m(z) + \mathbf{A}_{m-1}\underline{I}_{m-1}(z) = 0 \tag{12}$$

where the A's are matrices related to the structural as well as the incident parameters, and the I's are unknown vectors containing the amplitudes of the plane waves. The condition for the existence of nontrivial solutions of the last equation requires the vanishing of the coefficient matrix, and this defines the dispersion relation of the waveguiding structure. Such a three-term recurrence relation may be analyzed by the method of continued fractions with matrix elements. We have implemented a computer code for such a method; thus, the numerical analysis for the present problem can be carried out efficiently, and the results thus obtained are given in Section IV.

IV. Numerical Results and Discussions

Based on the exact formulation described in Section III, we are now in a position to carry out both qualitative and quantitative analyses of guiding characteristics of the 2-D periodic impedance surface. First, we shall invoke the concept of small perturbation to develop approximation techniques by which the first-order solutions can be constructed conveniently. This allows us to identify in an easy manner various physical effects associated with the structure in hand, and this will be particularly useful for practical design considerations. Second, for a numerical analysis, the infinite system of equations for the Fourier amplitudes has to be truncated to a finite order, and the numerical accuracy has to be carefully studied. After the numerical accuracy is assured, extensive numerical data are systematically obtained to identify all possible physical processes associated with the structure under investigation. Finally, the numerical data are displayed graphically in the form of the Brillouin diagram for physical interpretations.

A. Phase Diagram (k_x–k_y Relation)

In the analysis of the guiding characteristics of the 2-D periodic impedance surface at a given frequency, we may fix one component of the propagation vector, say k_x, and determine the other k_y or vice versa. Before embarking on elaborate computations, we first present a simple perturbation procedure to obtain approximate results with ease. In the absence of the periodic perturbations in (1), we have a uniform impedance surface for which the guiding characteristics are well known. In particular, for a lossless reactive surface, the propagation constant of the surface wave is given explicitly by

$$k_{sw}^2 = k_x^2 + k_y^2 = k_o^2 n_{sw}^2 \tag{13}$$

$$n_{sw}^2 = \begin{cases} 1 + \dfrac{1}{X_s^2}, & \text{for TE mode with } X_s < 0 \\ 1 + X_s^2, & \text{for TM mode with } X_s > 0 \end{cases} \tag{14}$$

where X_s is the surface reactance normalized to the free-space wave impedance $Z_o = 120\pi\,\Omega$. n_{sw} may be interpreted as the effective refractive index of the surface wave. It is noted that the TE surface wave exists only for capacitive surface, and the TM surface wave for inductive surface. In such a special case, the dispersion curve representing the relationship between k_x and k_y is a circle of the radius k_{sw}.

In the presence of the periodic perturbations on the surface impedance, all the space harmonics are generally excited with the propagation constants k_{xm} and k_{ym}, for $m, n = \cdots, -2, -1, 0, 1, 2, \cdots$, as defined in (6b) and (6c). From (A19) and (A20), it is straightforward to show that in the limit of vanishing perturbation, every space harmonic must satisfy approximately the same dispersion relation

$$\left(k_x + m\frac{2\pi}{a}\right)^2 + \left(k_y + n\frac{2\pi}{b}\right)^2 = k_{sw}^2 \tag{15}$$

where k_{sw} is, again, the propagation constant of the surface wave. Equation (13) represents a circle of the radius k_{sw}, centered at $(-2m\pi/a, -2n\pi/b)$, for any set of integers m and n ranging from the negative to positive infinity. For simplicity, these circles will be referred to as the unperturbed dispersion curves.

According to the theory of mode coupling, the dispersion root of the periodically perturbed structure may differ only slightly from that of the unperturbed one, but the propagation characteristics may change qualitatively from a propagating to a decaying wave in the stopband region. To illustrate the effect of the periodic modulation on the guiding characteristics of the reactive surface, we have carried out a parametric study on the dispersion curves under various operating conditions.

Fig. 2 shows the dispersion curves for the case of the impedance $Z_s = jZ_o$; the periods $a = b = 0.4243\lambda$, where λ is the free-space wavelength; and the modulation indexes $\delta_x = \delta_y = \delta_{xy} = 0.05$. Fig 2(a) shows the computed propagation constant k_y for a given real k_x, while Fig. 2(b)

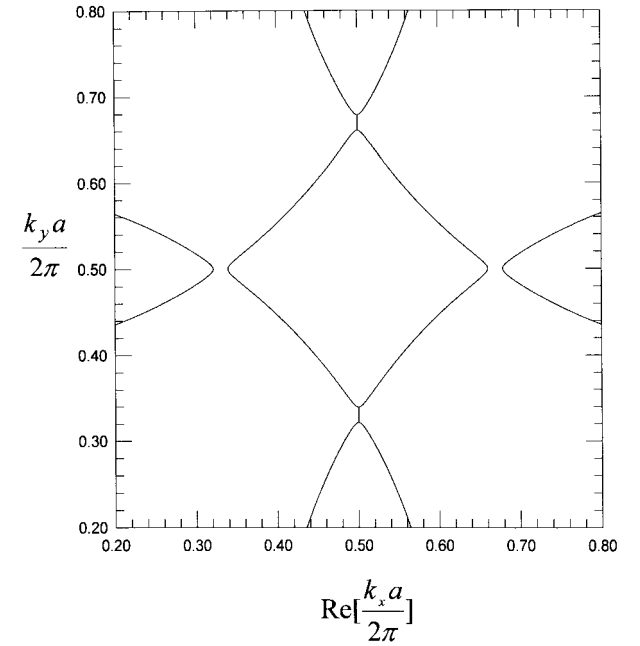

(a)

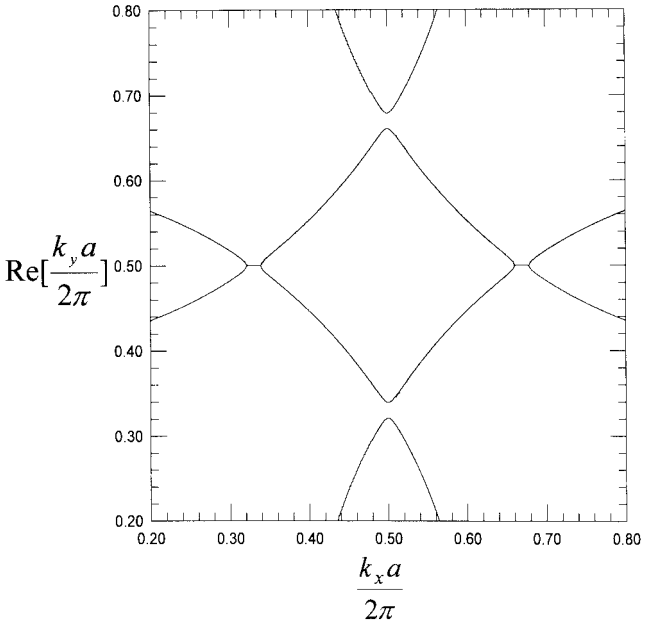

(b)

Fig. 2. Dispersion curves for the case of $X_s = jZ_0$, $\delta_x = \delta_y = \delta_{xy} = 0.05$ and $a = b = 0.424\,264\lambda$. (a) Computation of k_x for given k_y. (b) Computation of k_y for given k_x.

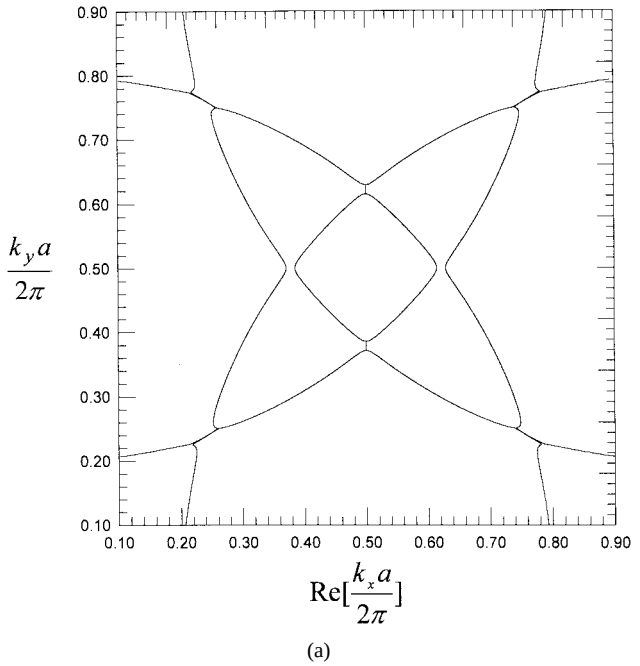

(a)

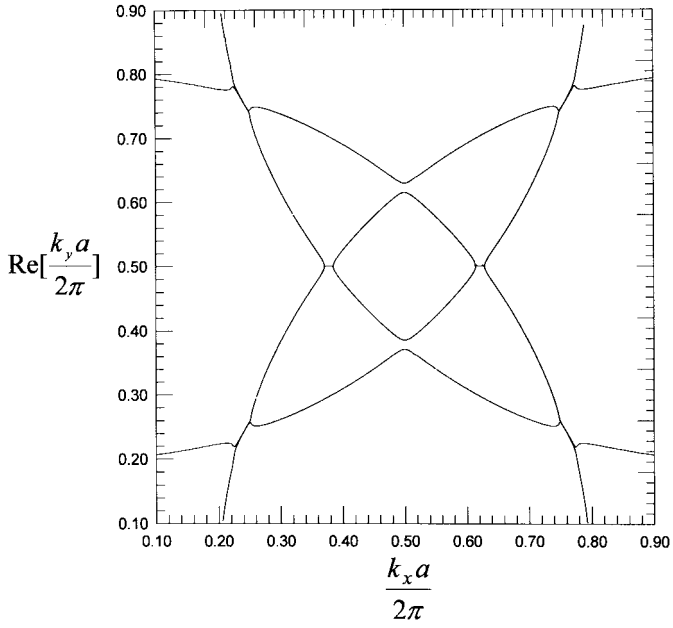

(b)

Fig. 3. Dispersion curves for the case of $X_s = jZ_0$, $\delta_x = \delta_y = \delta_{xy} = 0.05$ and $a = b = 0.5657\lambda$. (a) Computation of k_x for given k_y. (b) Computation of k_y for given k_x.

shows the computed propagation constant k_x for a given real k_y. For the low-frequency operation, the normalized radius of each circle $(k_{sw}a/2\pi)$ is intentionally set to be smaller than $1/\sqrt{2}$ so that the intersections occur only between the circles centered along either the k_x- or k_y-axis, but not between those along the diagonal directions. The implication of these diagrams is that the 2-D periodic structure behaves like a 1-D one in either the x- or y-directions.

On the other hand, at higher frequencies, k_{sw} becomes larger, and additional interactions may take place between the circles centered along the diagonal directions. In Fig. 3, the radius of the circles is increased to allow the interactions between (0, 0) and $(-1, -1)$ harmonics and also between $(-1, 0)$ and $(0, -1)$ harmonics to occur. Here, the four stopbands in the central portion are the same as those in the low-frequency case shown in Fig, 2, while the four extra stopbands that are slanted at an angle with respect to the k_x-axis are generated. As will become clearer later on, these extra stopbands are mainly due to the cross modulation term containing δ_{xy}. Inside these slanted stopbands, k_y is complex for a given real k_x, and so is k_x for a given real k_y. These extra stopbands provide

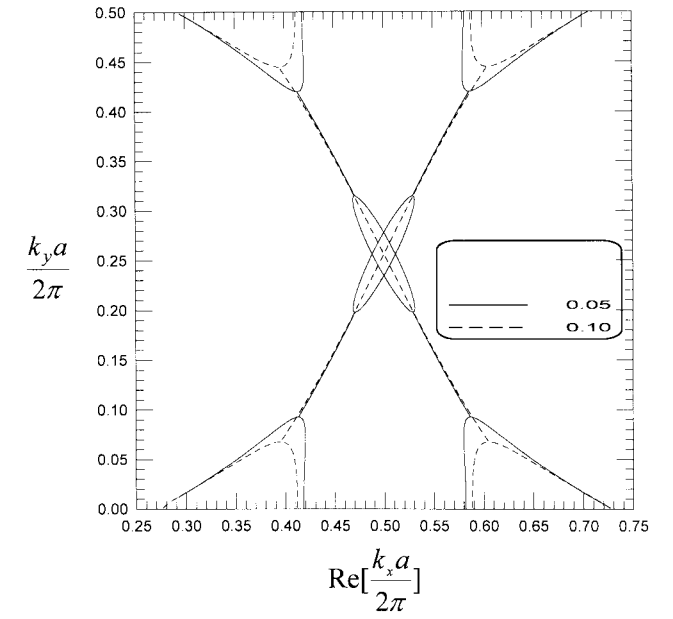

(a)

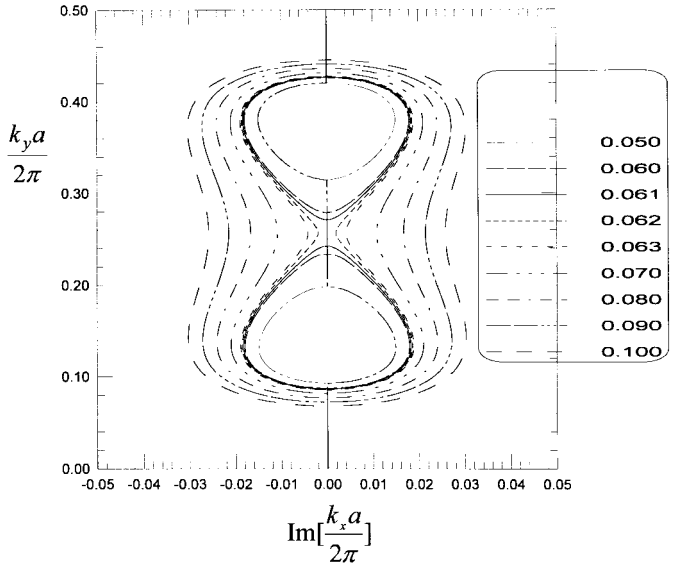

(b)

Fig. 4. Stopband behavior with the modulation index as a parameter for the case $X_s = jZ_0$, $\delta_x = \delta_y = 0$, $a = 0.41\lambda$ and $b = 0.81\lambda$. (a) Compute real part of k_x for given k_y. (b) Compute imaginary part of k_x for given k_y.

additional incident conditions for the suppression of surface waves, if needed.

To further understand the characteristics of the extra (slanted) stopbands, Fig. 4 shows the change in the bandwidth as the modulation index δ_{xy} is increased. Fig. 4(a) shows the real part of k_x as a function of k_y for two values of δ_{xy}, while Fig. 4(b) shows the imaginary part for seven values of δ_{xy}. Evidently, the bandwidth of each of the four stopbands increases with increasing δ_{xy}; eventually, they merge together to become two large ones. From the values of k_x and k_y at the band edges for the case of $\delta_{xy} = 0.1$, it is estimated that the guided wave stays within the stopband for the incident angle ranging from 6.2° to 48.4°, as measured from the x-axis. As a conjecture, a 2-D periodic array of metal patches is expected to have large modulation indexes, and this may explain the wide-angle suppression of surface wave by using the class of metal structures.

B. Brillouin Diagram

Another useful way of investigating the waveguiding phenomenon is to plot the relationship between k_x and k_o for a given k_y or between k_y and k_o for a given k_x. As an example, consider the case where a 2-D periodic impedance surface is connected to a uniform impedance surface at $x = 0$ (along the y-axis), and a surface wave is incident obliquely at the incident angle ϕ_{inc} from the uniform impedance surface, as shown in Fig. 1(b). Here, by fixing the incident angle, k_y is determined for a given frequency and we can look for the dispersion root of k_x. This is done over a range of frequency to construct the k_o–k_x diagram or the Brillouin diagram. In the case of a 1-D periodic structure that is uniform along the y-direction, we have only a fixed k_y; on the other hand, in the 2-D case, there exist many harmonics with different wavenumbers k_{yn} for any positive or negative integer n. From (15), the unperturbed dispersion curves are plotted in Figs. 5(a) and 6 for two different incident angles. It is noted that the unperturbed dispersion curves for the fundamental ($n = 0$) harmonic are straight lines, as in the case of 1-D periodic structure, while the new ones for $n \neq 0$ are hyperbolic curves, which are present only in the case of 2-D periodic structures. Again, from the coupled-mode theory, the dispersion curves for the case of small perturbation should follow these unperturbed curves, except in the vicinities of the intersection points, as circled and marked by A, B, C, etc., in Figs. 5(a) and 6. Here, the number in the parentheses after each character stands for the frequency at which the intersection occurs. Looking at Fig. 5(a), we can identify two types of wave interactions: co-flow interaction at the point marked by D and the contra-flow interaction at all other points. The locations of these intersections will be used as the reference points for our numerical as well as physical analysis.

It is well known that in the case of a 1-D periodic structure [3], there exist bound-wave regions in the form of a triangle, known as the bound-wave triangle. Physically, if a dispersion curve falls within the triangles in a frequency range, the wave guided by the structures is always bound over the frequency range; otherwise the guided wave may radiate its energy into the air region. The bound-wave region is a simple triangle for the case of a 1-D periodic structure, but it may be changed in the 2-D case.

To better understand the bound-wave region, we recall that the longitudinal propagation constant k_{zmn} of the mnth harmonic in the air region is given by

$$k_{zmn} = \sqrt{k_0^2 - k_{tmn}^2} \tag{16}$$

with

$$k_{tmn}^2 = \left(k_x + m\frac{2\pi}{a}\right)^2 + \left(k_y + n\frac{2\pi}{b}\right)^2. \tag{17}$$

For k_{tmn}^2 smaller than k_0^2, the space harmonic will propagate from the impedance surface in the air region and a guided wave

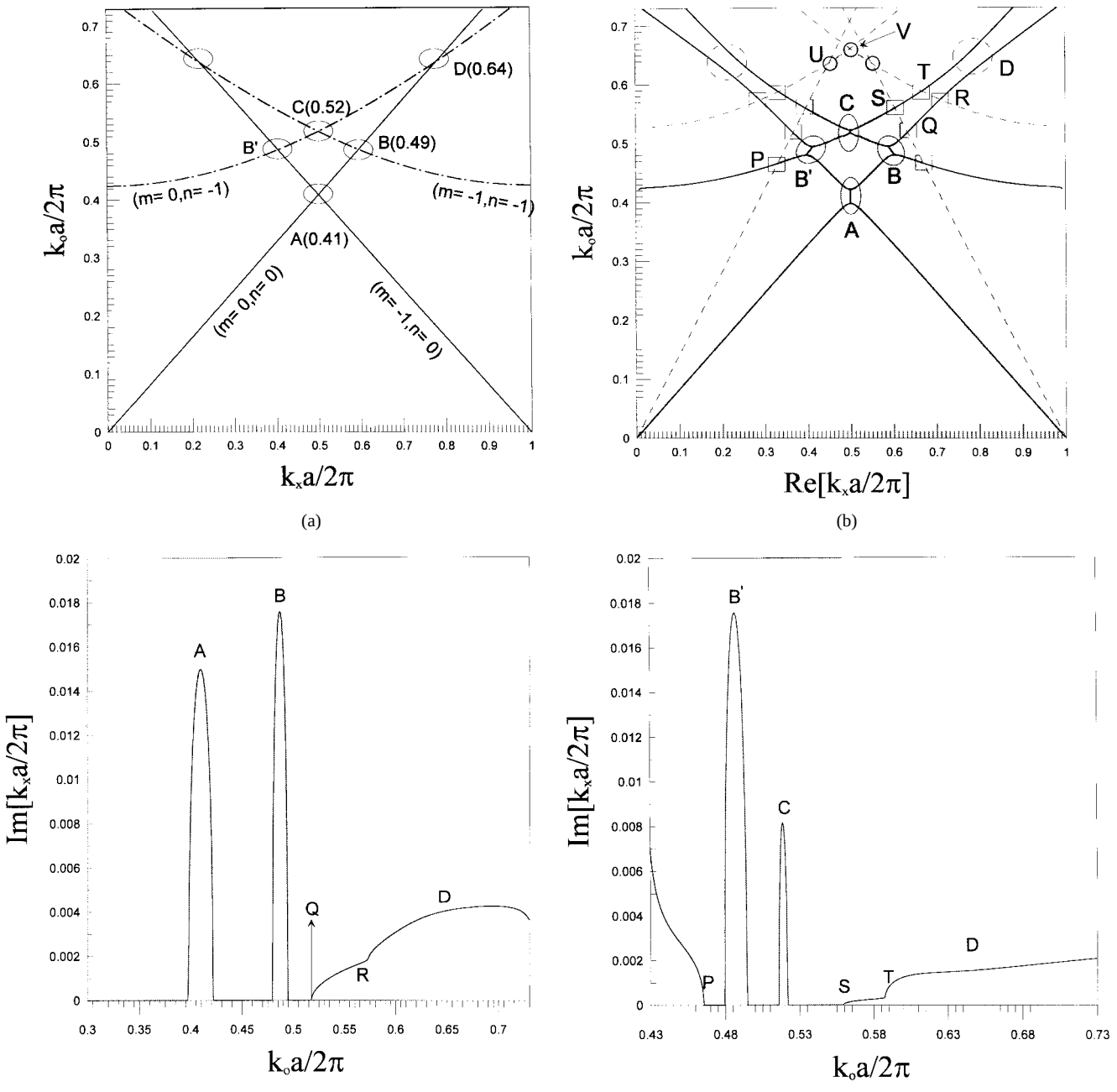

Fig. 5. (a) Brillouin diagram of an impedance surface: unperturbed dispersion curves. (b) Brillouin diagram of a 2-D periodic impedance surface. (c) Variation of the attenuation parameter with normalized frequency $k_o a/2\pi$ for the same impedance surface as that in Fig. 5(b). (d) Variation of the attenuation parameter with normalized frequency $k_o a/2\pi$ for the same impedance surface as flat in Fig. 5(b).

will lose its energy as it propagates. Therefore, the boundary of the bound-wave region is defined by

$$\left(k_x + m\frac{2\pi}{a}\right)^2 + \left(k_y + n\frac{2\pi}{b}\right)^2 = k_0^2. \tag{18}$$

With $k_y = k_o n_{sw} \sin\phi_{\text{inc}}$, the bound-wave region is shown with a highlighted area in Fig. 5(b) for $\phi_{\text{inc}} = 30°$ and in Fig. 6 for $\phi_{\text{inc}} = 50°$. It is noted that in the latter case, we have k_y always greater than k_o; thus, the bound-wave region is determined by the higher harmonic, $n = -1$, not the fundamental one.

Fig. 5(b) shows the Brillouin diagram for a modulated inductive surface for a TM guided wave for the case of the impedance $Z_s = jZ_o$, the periods $a/b = 0.9$, and the modulation index $\delta_x = \delta_y = 0.1$ and $\delta_{xy} = 0.05$. Evidently, the diagram is horizontally symmetrical with respect to the middle line $(k_x a/2\pi)$; therefore, we may concentrate on the second half of the diagram. Comparing Fig. 5(a) and (b), we observe that the actual dispersion curves closely follow the unperturbed ones, and strong interactions or couplings take place around the intersection points marked by circles in both diagrams. Also shown in Fig. 5(b) is the highlighted area for the bound-wave region. Inside the bound-wave region, we

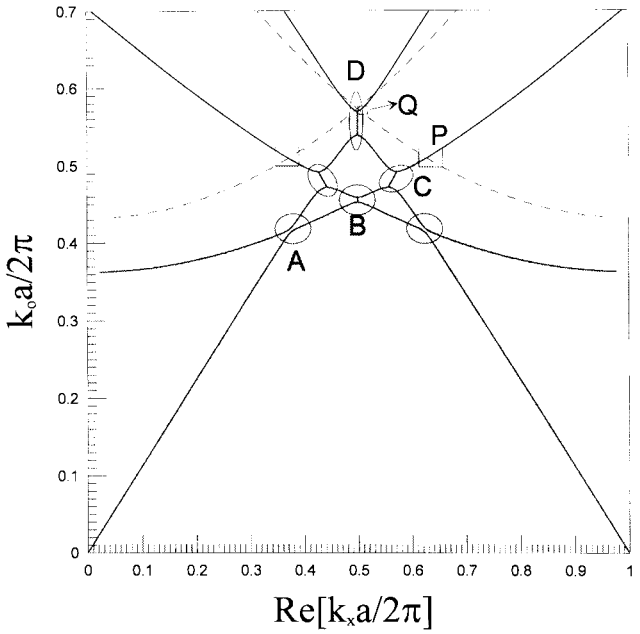

Fig. 6. Brillouin diagram of a 2-D periodic impedance surface.

have three distinct stopbands, as marked by A, B, and C. In comparison with Fig. 5(a), we see that the stopband marked by A is due to the interactions between the space harmonics in the x-direction, ($m = 0$, $n = 0$) and ($m = -1$, $n = 0$). Similarly, the one marked by C is due to the interactions between the space harmonics ($m = 0$, $n = -1$) and ($m = -1$, $n = -1$). On the other hand, the one marked by B is due to the interactions between space harmonics in both the x- and y-directions ($m = 0$, $n = 0$) and ($m = -1$, $n = -1$). In the portion outside the bound-wave region in Fig. 5(b), a strong co-flow interaction is evident in the area marked by D. The intersection points of the dispersion curves with the boundaries of the bound-wave region are enclosed by a square. These boundary points physically means the beginning and ending of the leaky-wave phenomenon, and are convenient for physical interpretations of the numerical results obtained herein.

Still referring to Fig. 5(b), we follow the dispersion curve of the fundamental harmonic ($m = 0$, $n = 0$), starting from the point O through A, B, Q, R, then to the point D. The attenuation constant $\mathrm{Im}[k_x a/2\pi]$ against the frequency is plotted in Fig. 5(c), with the range of bound-wave highlighted. Inside the bound-wave region, there are two distinct stopbands marked by A and B, as in Fig. 5(b). These stopbands in the low-frequency range are surrounded by pure passbands in which the attenuation constant vanishes. Beyond the point Q, the dispersion root is generally complex because the frequency is so high that the fundamental harmonic is radiating. It is interesting to note that the point R is at the onset of radiation of the harmonic ($m = -1$, $n = -1$); thus, a second beam starts to appear and the attenuation constant increases substantially. In the region of co-flow interaction, as indicated by D, no substantial change in the attenuation constant occurs. Similar results are obtained for the other branch of the dispersion curves, as marked by the points P, B', C, S, and T, and as plotted in Fig. 5(d). In contrast, the branch starts in a leaky-wave region and falls in the bound-wave region over a range of frequency, before entering again into another leaky-wave region. An interesting phenomenon is that in the range of co-flow interactions, as marked by D, the decay constant here is very much different from that in the corresponding range in Fig. 5(c), even though the coupling between the two modes is very strong.

To see the effect of the incident angle on the guidance characteristics, we consider here the case of the incident angle $\phi_{\mathrm{inc}} = 50°$. The results are shown in Fig. 6. In this case, k_y is about equal to $1.083k_o$, always larger than k_o; therefore, for the fundamental harmonic in the y-direction, $n = 0$, the space harmonic (m, 0) is always below cutoff. In this case, the bound-wave region is dictated by the second space harmonic in the y-direction, as determined by (18). For completeness, the dispersion curves of the lowest three space harmonics in the y-direction are shown here, together with the highlighted area for the bound-wave region. The general behaviors of the attenuation constant as a function of frequency are similar to those in Fig. 5(c) and (d) and, for succinctness, are not shown. However, Fig. 6 contains a very important message that the periodic variation may give rise to unexpected radiation.

V. Conclusions

We have presented a rigorous treatment of guided waves on the planar 2-D periodic impedance surface. Numerical results are systematically carried out and are displayed in the form of the Brillouin diagram to identify the types of wave interactions and to show the stopband structure of the dispersion curves. Particular attention is paid to the new phenomena that arise in the case of 2-D periodic structures, but not in the 1-D case. At a sufficiently high frequency, there exist extra stopbands that provide more degrees of freedom for the design of microwave and millimeter-wave circuits and antennas, such as the suppression of leaky surface waves. In the case of large modulation indexes, we have observed for the first time a drastic change within the stopband, including the merge of neighboring stopbands. Most importantly, the additional periodicity in the y-direction may results in unexpected leaky waves in 2-D periodic structures. The practical implication of these new phenomena remains to be explored for new applications.

Appendix

Since the tangential electric and magnetic fields in the air should be expressed as a superposition of (3) and (4), we have

$$\underline{z}_o \times \underline{E}(\underline{\rho}, z) = \sum_{m,n} \left[\underline{a}'_{mn} \cdot V'_{mn}(z) + \underline{a}''_{mn} \cdot V''_{mn}(z)\right] \cdot \varphi_{mn} \tag{A1}$$

$$\underline{H}(\underline{\rho}, z) = \sum_{m,n} \left[\underline{a}'_{mn} \cdot I'_{mn}(z) + \underline{a}''_{mn} \cdot I''_{mn}(z)\right] \cdot \varphi_{mn} \tag{A2}$$

$$\varphi_{mn} = \exp(-\underline{k}_{tmn} \cdot \underline{\rho}).$$

By substituting (A1) and (A2) into (11), we obtain

$$\begin{aligned}\sum_{m,n}\left[V'_{mn}(0)\underline{a}'_{mn}+V''_{mn}(0)\underline{a}''_{mn}\right]\exp(-\underline{k}_{tmn}\cdot\underline{\rho})\\ =Z_s\sum_{m,n}\Bigg\{\left[I'_{mn}(0)\underline{a}'_{mn}+\underline{I}''_{mn}(0)\underline{a}''_{mn}\right]\\ +\delta_x\left[I'_{m-1,n}(0)\underline{a}'_{m-1,n}+I''_{m-1,n}(0)\underline{a}''_{m-1,n}\right]\\ +\delta_x\left[I'_{m+1,n}(0)\underline{a}'_{m+1,n}+I''_{m+1,n}(0)\underline{a}''_{m+1,n}\right]\\ +\delta_y\left[I'_{m,n-1}(0)\underline{a}'_{m,n-1}+I''_{m,n-1}(0)\underline{a}''_{m,n-1}\right]\\ +\delta_y\left[I'_{m,n+1}(0)\underline{a}'_{m,n+1}+I''_{m,n+1}(0)\underline{a}''_{m,n+1}\right]\\ +\delta_{xy}\Big[I'_{m-1,n-1}(0)\underline{a}'_{m-1,n-1}\\ \quad+I''_{m-1,n-1}(0)\underline{a}''_{m-1,n-1}\Big]\\ +\delta_{xy}\Big[I'_{m-1,n+1}(0)\underline{a}'_{m-1,n+1}\\ \quad+I''_{m-1,n+1}(0)\underline{a}''_{m-1,n+1}\Big]\\ +\delta_{xy}\Big[I'_{m+1,n-1}(0)\underline{a}'_{m+1,n-1}\\ \quad+I''_{m+1,n-1}(0)\underline{a}''_{m+1,n-1}\Big]\\ +\delta_{xy}\Big[I'_{m+1,n+1}(0)\underline{a}'_{m+1,n+1}\\ \quad+I''_{m+1,n+1}(0)\underline{a}''_{m+1,n+1}\Big]\Bigg\}\\ \cdot\exp(-\underline{k}_{t,mn}\cdot\underline{\rho}).\end{aligned}\tag{A3}$$

Taking the inner product of $\underline{a}'_{m,n}$ with both sides, the voltage and current amplitude has the following relation:

$$\begin{aligned}V'_{m,n}(0)=Z_s\sum_{m,n}\Bigg\{I'_{mn}(0)+\delta_x\Big[K^{(1,1)}_{m-1,n}I'_{m-1,n}(0)\\ \quad+K^{(1,2)}_{m-1,n}I''_{m-1,n}(0)\Big]\\ +\delta_x\left[K^{(1,1)}_{m+1,n}I'_{m+1,n}(0)+K^{(1,2)}_{m+1,n}I''_{m+1,n}(0)\right]\\ +\delta_y\left[K^{(1,1)}_{m,n-1}I'_{m,n-1}(0)+K^{(1,2)}_{m,n-1}I''_{m,n-1}(0)\right]\\ +\delta_y\left[K^{(1,1)}_{m,n+1}\underline{I}'_{m,n+1}(0)+K^{(1,2)}_{m,n+1}\underline{I}''_{m,n+1}(0)\right]\\ +\delta_{xy}\Big[K^{(1,1)}_{m-1,n-1}I'_{m-1,n-1}(0)\\ \quad+K^{(1,2)}_{m-1,n-1}I''_{m-1,n-1}(0)\Big]\\ +\delta_{xy}\Big[K^{(1,1)}_{m-1,n+1}I'_{m-1,n+1}(0)\\ \quad+K^{(1,2)}_{m-1,n+1}I''_{m-1,n+1}(0)\Big]\\ +\delta_{xy}\Big[K^{(1,1)}_{m+1,n-1}I'_{m+1,n-1}(0)\\ \quad+K^{(1,2)}_{m+1,n-1}I''_{m+1,n-1}(0)\Big]\\ +\delta_{xy}\Big[K^{(1,1)}_{m+1,n+1}I'_{m+1,n+1}(0)\\ \quad+K^{(1,2)}_{m+1,n+1}I''_{m+1,n+1}(0)\Big]\Bigg\}\end{aligned}\tag{A4}$$

with $m, n=-\infty\cdots+\infty$, where

$$K^{(1,1)}_{m\pm1,n\pm1}=\langle\underline{a}'_{m,n}|\underline{a}'_{m\pm1,n\pm1}\rangle\tag{A5}$$

and

$$K^{(1,2)}_{m\pm1,n\pm1}=\langle\underline{a}'_{m,n}|\underline{a}''_{m\pm1,n\pm1}\rangle.\tag{A6}$$

We may now fix the integer m and group the harmonics according to the index n to form the new vector relationship

$$\begin{aligned}Y_s\underline{V}'_m(0)=&\mathbf{D}^{(1,1)}_m\underline{I}'_m(0)+\mathbf{K}^{(1,1)}_{m+1}\underline{I}'_{m+1}(0)\\ &+\mathbf{K}^{(1,1)}_{m-1}\underline{I}'_{m-1}(0)+\mathbf{X}^{(1,2)}_m\underline{I}''_m(0)\\ &+\mathbf{K}^{(1,2)}_{m+1}\underline{I}''_{m+1}(0)+\mathbf{K}^{(1,2)}_{m-1}\underline{I}''_{m-1}(0).\end{aligned}\tag{A7}$$

Taking the inner product of $\underline{a}''_{m,n}$ in (A3) with both sides and performing the same process as the above, we obtain

$$\begin{aligned}Y_s\underline{V}''_m(0)=&\mathbf{D}^{(2,2)}_m\underline{I}''_m(0)+\mathbf{K}^{(2,2)}_{m+1}\underline{I}''_{m+1}(0)\\ &+\mathbf{K}^{(2,2)}_{m-1}\underline{I}''_{m-1}(0)+\mathbf{X}^{(2,1)}_m\underline{I}'_m(0)\\ &+\mathbf{K}^{(2,1)}_{m+1}\underline{I}'_{m+1}(0)+\mathbf{K}^{(2,1)}_{m-1}\underline{I}'_{m-1}(0).\end{aligned}\tag{A8}$$

where $\underline{V}'_m(0)$, $\underline{I}'_m(0)$, and $\underline{I}''_m(0)$ are column vectors with $V_{mn}(0)$ and $I_{mn}(0)$ as their nth elements, respectively, and matrices $D^{(1,1)}_m$, $X^{(1,2)}_m$, $K^{(1,1)}_{m\pm1}$, and $K^{(1,2)}_{m\pm1}$ may be defined as

$$\mathbf{D}^{(i,j)}_m=\begin{pmatrix}\ddots&&&\\ &1&\delta_y k^{(i,j)}_{m,n-1}&0\\ &\delta_y k^{(i,j)}_{m,n+1}&1&\delta_y k^{(i,j)}_{m,n-1}\\ &0&\delta_y k^{(i,j)}_{m,n+1}&1\\ &&&\ddots\end{pmatrix}\tag{A9}$$

$$\mathbf{X}^{(i,j)}_m=\begin{pmatrix}\ddots&&&\\ &0&\delta_y k^{(i,j)}_{m,n-1}&0\\ &\delta_y k^{(i,j)}_{m,n+1}&0&\delta_y k^{(i,j)}_{m,n-1}\\ &0&\delta_y k^{(i,j)}_{m,n+1}&0\\ &&&\ddots\end{pmatrix}\tag{A10}$$

$$\mathbf{K}^{(i,j)}_{m\pm1}=\begin{pmatrix}\ddots&&&\\ &\delta_x k^{(i,j)}_{m\pm1,n}&\delta_{xy}k^{(i,j)}_{m\pm,n-1}&0\\ &\delta_{xy}k^{(i,j)}_{m\pm1,n+1}&\delta_x k^{(i,j)}_{m\pm1,n}&\delta_{xy}k^{(i,j)}_{m\pm1,n-1}\\ &0&\delta_{xy}k^{(i,j)}_{m\pm1,n+1}&\delta_x k^{(i,j)}_{m\pm1,n}\\ &&&\ddots\end{pmatrix}\tag{A11}$$

where $i, j=1, 2$.

Equations (A7) and (A8) could be rearranged and expressed as a super matrix and vector form with the following notations:

$$Y_s\underline{V}_m(0)=\mathbf{A}_{m+1}\underline{I}_{m+1}(0)+\mathbf{D}_m\underline{I}_m(0)+\mathbf{A}_{m-1}\underline{I}_{m-1}(0)\tag{A12}$$

where

$$\mathbf{A}_{m\pm1} = \begin{pmatrix} \mathbf{K}_{m\pm1}^{(1,1)} & \mathbf{K}_{m\pm1}^{(1,2)} \\ \mathbf{K}_{m\pm1}^{(2,1)} & \mathbf{K}_{m\pm1}^{(2,2)} \end{pmatrix} \tag{A13}$$

$$\mathbf{D}_{m} = \begin{pmatrix} \mathbf{D}_{m}^{(1,1)} & \mathbf{X}_{m}^{(1,2)} \\ \mathbf{X}_{m}^{(2,1)} & \mathbf{D}_{m}^{(2,2)} \end{pmatrix} \tag{A14}$$

$$\underline{V}_m(0) = \begin{pmatrix} \underline{V}'_m(0) \\ \underline{V}''_m(0) \end{pmatrix} \tag{A15}$$

$$\underline{I}_m(0) = \begin{pmatrix} \underline{I}'_m(0) \\ \underline{I}''_m(0) \end{pmatrix}. \tag{A16}$$

In the absence of the incident wave, the relationship between $\underline{V}_m(0)$ and $\underline{I}_m(0)$ will be written as

$$\underline{V}_m(0) = -\mathbf{Z}_m^{(a)} \underline{I}_m(0) \tag{A17}$$

where

$$\mathbf{Z}_m^{(a)} = \begin{pmatrix} \mathbf{Z}_m^{\prime(a)} & 0 \\ 0 & \mathbf{Z}_m^{\prime\prime(a)} \end{pmatrix}. \tag{A18}$$

$Z_m^{\prime(a)}$ and $Z_m^{\prime\prime(a)}$ are the diagonal matrices with $Z_{m,n}^{\prime(a)}$ and $Z_{m,n}^{\prime\prime(a)}$ as their nth element, respectively.

By substituting (A17) into (A12), we obtain the three-term recurrence relation

$$\mathbf{A}_{m+1}\underline{I}_{m+1}(0)+\mathbf{B}_m\underline{I}_m(0)+\mathbf{A}_{m-1}\underline{I}_{m-1}(0) = 0 \tag{A19}$$

where

$$\mathbf{B}_m = \mathbf{D}_m + Y_s\mathbf{Z}_m^{(a)}. \tag{A20}$$

REFERENCES

[1] T. Tamir, H. C. Wang, and A. A. Oliner, "Wave propagation in sinusoidally stratified dielectric media," *IEEE Trans. Microwave Theory Tech.*, vol. MTT-12, p. 323, May 1964.

[2] A. Hessel and A. A. Oliner, "A new theory of Wood's anomalies on optical gratings," *Appl. Opt.*, vol. 4, pp. 1275–1297, 1965.

[3] S. T. Peng, T. Tamir, and H. L. Bertoni, "Theory of dielectric grating waveguides," *IEEE Trans. Microwave Theory Tech.*, vol. MTT-23, pp. 123–133, Jan. 1975.

[4] C. Elach, "Wave in active and passive periodic structures: A review," *Proc. IEEE*, vol. 64, pp. 1666–1698, Dec. 1976.

[5] S. T. Peng, "Rigorous formulation of scattering and guidance by dielectric grating waveguides: General case of oblique incidence," *J. Opt. Soc. Amer.*, vol. 6, pp. 1869–1883, 1989.

[6] S. T. Peng and M. J. Shiau, "Scattering of plane waves by corrugated dielectric layers," presented at the Int. URSI Symp. Electromag. Waves, Satiago de Compostela, Spain, 1983.

[7] S. T. Peng, "Rigorous analysis of guided waves in doubly periodic structures," *J. Opt. Soc. Amer.*, vol. 6, pp. 1448–1456, 1990.

[8] T. K. Gaylord and M. G. Moharam, "Analysis and applications of optical diffraction by gratings," *Proc. IEEE*, vol. 73, pp. 884–937, Oct. 1985.

[9] R. C. Hall, R. Mittra, and K. M. Mitzner, "Analysis of multilayered periodic structures using generalized scattering matrix theory," *IEEE Trans. Antennas Propagat.*, vol. 36, pp. 511–517, Apr. 1988.

[10] D. Maystre, "Electromagnetic study of photonic band gaps," *Pure Appl. Opt.*, vol. 3, no. 6, pp. 975–993, Nov. 1994.

[11] H. Y. D. Yang, "Finite difference analysis of 2-D photonic crystals," *IEEE Trans, Microwave Theory Tech.*, vol. 44, pp. 2688–2695, Dec. 1996.

[12] H. Y. D. Yang, J. A. Castaneda, and N. G. Alexopoulos, "An integral equation analysis of an infinite array of rectangular dielectric waveguides," *IEEE Trans. Microwave Theory Tech.*, vol. 38, pp. 873–880, July 1990.

[13] V. Radisic, Y. Qian, R. Coccioli, and T. Itoh," Novel 2-D photonic bandgap structure for microstrip lines," *IEEE Microwave Guided Wave Lett.*, vol. 8, pp. 69–71, Feb. 1998.

[14] Y. Qian, V. Radisic, and T. Itoh, "Simulation and experiment of photonic bandgap structures for microstrip circuits," in *Proc. APMC*, Hong Kong, Dec. 1997, pp. 585–588.

[15] V. Radisic, Y. Qian, and T. Itoh, "Broad-band power amplifier using dielectric photonic bandgap structure," *IEEE Microwave Guided Wave Lett.*, vol. 8, pp. 13–14, Jan. 1998.

[16] M. P. Kesler, J. G. Maloney, and B. L. Shirly, "Antenna design with the use of photonic bandgap materials as all dielectric planar reflectors," *Microwave Opt. Technol. Lett.*, vol. 11, no. 4, pp. 169–174, 1996.

[17] T. J. Ellis and G. M. Rebeiz, "MM-wave tapered slot antennas on micromachined photonic bandgap dielectrics," in *IEEE MTT-S Int. Microwave Symp. Dig.*, June 1996, pp. 1157–1160.

[18] R. B. Hwang and S. T. Peng, "Performance evaluation of bigrating as a beam splitter," *Appl. Opt.*, vol. 36, no. 10, pp. 2011–2018, 1997.

[19] ———, "Plane wave scattering by bigratings," presented at the IEEE AP-S Int. Symp. URSI North Amer. Radio Sci. Meeting, Montreal, P.Q., Canada, July 13–18, 1997.

[20] S. T. Peng and R. B. Hwang, "Analysis of plane-wave scattering by bigratings," presented at the Int. Conf. Microwave Millimeter Wave Technol., Beijing, China, Aug. 18–20, 1998.

[21] S. T. Peng, "Guided waves on 2D periodic structures and their relation to planar photonic band gap structures," presented at the APMC Workshop New Propagation Phenomena Millimeter-Wave Planar Circuits/Lines Applicat., 1998, Yokohama, Japan.

Ruey Bing Hwang (S'95–M'96) was born in Nan-Tou, Taiwan, R.O.C., on January 20, 1967. He received the B.S. degree in communication engineering from the National Chaio-Tung University, Hsinchu, Taiwan, R.O.C., in 1990, the M.S. degree from the Institute of Electrical Engineering, National Taiwan University, Taipei, Taiwan, R.O.C., in 1992, and the Ph.D. degree from the Institute of Electronics, National Chaio-Tung University, Hsinchu, Taiwan, R.O.C., in 1996.

From 1996 to 1999, he was with the National Center for High-Performance Computing, Hsinchu, Taiwan, R.O.C, where he was involved with computational electromagnetic. In the summer of 1999, he joined the Microelectronics and Information Systems Research Center, National Chaio-Tung University, Hsinchu, Taiwan, R.O.C., as an Associated Researcher. His professional interests include guidance and scattering characteristics of periodic structures, antenna design, and electromagnetic compatibility.

Dr. Hwang is a member of Phi Tau Phi.

Song Tsuen Peng (M'74–SM'82–F'88) was born in Taiwan, R.O.C., on February 19, 1937. He received the B.S. degree in electrical engineering from the National Cheng Kung University, Hsinchu, Taiwan, R.O.C., in 1959, the M.S. degree in electronics from the National Chiao-Tung University, Hsinchu, Taiwan, R.O.C., in 1961, and the Ph.D. degree in electro-physics from the Polytechnic Institute of Brooklyn, Brooklyn, NY, in 1968.

Following 1968, he held various research positions with the Polytechnic Institute of Brooklyn. From 1983 to 1990, he was a Professor of electrical engineering and Director of the Electromagnetics Laboratory, New York Institute of Technology, Old Westbury. Since 1991, he has been a Professor of Communication Engineering at the National Chiao-Tung University. Since September 1998, he has been the Director of the Microelectronics and Information Systems Research Center, National Chaio-Tung University. He has been active in the field of general waveguiding structures and has published numerous papers on electromagnetics, optics, and acoustics. His current research interests include the guidance and scattering characteristics of periodic structures, antenna design, and electromagnetic compatibility.

Dr. Peng is a member of Sigma Xi.